Measurement of Aerodynamic Forces on a NACA 0012 Airfoil

Gayathri Kola
The University of Texas at Arlington, Arlington, Texas, 76019, United States

In this experiment, a NACA 0012 axis-symmetric airfoil is characterized by forces acting on its upper and lower surfaces. The airfoil is tested in a low-speed, subsonic wind tunnel with pressure taps attached along both sides of the airfoil that measure the local pressure. These readings along with the freestream dynamic pressure reading from the analog manometer that is connected to the wind tunnel are used to calculate local pressure coefficients. The angle of attack of the airfoil is changed from 0° to 20° in 2° increments, rotated counterclockwise from the freestream velocity. The local pressure coefficients are used to obtain lift and drag coefficients for the corresponding angles of attack. The pressure distributions for the angle of attacks of 0°, 14°, and 20° are plotted against normalized chord to visualize pressure gradients at normal, stall point, and beyond stall regions. The maximum lift coefficient occurs at 14° with a value of 0.902. The Reynolds number is calculated and compared against the R&M 3726 document where a similar experiment was conducted with a higher Reynolds number. From the results, it is speculated that the obtained value maximum lift coefficient is much lower than R&M 3726 due to a much lower Reynolds number.

I. Nomenclature

ρ = density of air
α = angle of attack
y = y-distance from the chord line
x = x-distance from the leading edge
u = velocity
b = span
c = chord
T = room temperature
R = gas constant of air
P = room pressure
L = lift
D = drag
F = force
ρ_∞ = freestream density
U_∞ = freestream velocity
P_{total} = total pressure
P_{static} = static pressure
P_{scan} = pressure from differential pressure scanner
P_{pitot} = pressure from the pitot tube
P_{local} = local pressure
P_∞ = freestream pressure
C_L = lift coefficient
C_D = drag coefficient
C_{P_l} = local pressure coefficient
C_{P_U} = local pressure coefficient on the upper surface of the airfoil
C_{P_L} = local pressure coefficient on the lower surface of the airfoil

$C_{F_{y'}}$ = force coefficient on the y-direction
$C_{F_{x'}}$ = force coefficient on the x-direction

II. Introduction

Wind tunnels are used to mimic the flight conditions of an aircraft using a smaller, scaled prototype of its design and parts. Forces can be measured for these prototypes and their lift, drag characteristics can be noted. This allows for tangible, verifiable data along with flight tests. Additionally, Computation Fluid Dynamics (CFD) is often used to test the correctness of base assumptions before testing on a large wind tunnel. While CFD helps in obtaining a preliminary check of the flow conditions, the results must be verified using real-life experiments. A few near-ideal conditions such as flow uniformity and small turbulences can be recreated in wind tunnels, which is a feature of the AF100 low-speed subsonic wind tunnel used in this experiment. The experiment is focused on characterizing the axis-symmetric NACA 0012 airfoil connected with pressure taps along its upper and lower surfaces. These local pressure readings allow for the measurement of forces acting on the airfoil, namely the lift and drag forces. The pressure readings are recorded for the angle of attack ranging from 0° to 20° in 2° increments.

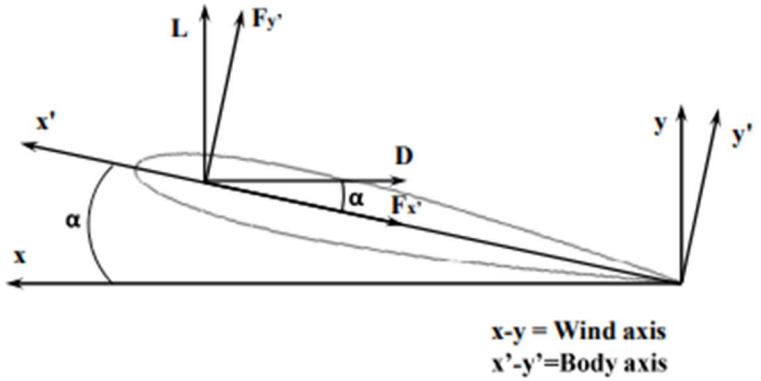

Fig. 1 Airfoil with wind and body axis systems [1].

Consider the airfoil at an angle of attack from the wind axis in Fig (1). There are two axis systems associated here, the wind axis and the body axis. The body axis is attached to the airfoil while the wind axis is concerned with the relative wind. The lift and drag forces measured on the airfoil will then become a function of the angle of attack and the body forces $F_{y'}$ (body normal force) and $F_{x'}$ (body axial force). The body surface forces encompass both, the pressure and shear distribution. To obtain the entire lift and drag forces, the local pressure and shear forces must be integrated along the upper and lower surfaces. However, in this experiment, the pressure scanners used are only capable of measuring the local pressure along the airfoil surface. Thus, the shear distributions are neglected from the analysis. With the local pressure data, the pressure drag can be calculated. Since the airfoil is symmetric and the testing conditions are for low-speed, low-turbulence, and flow uniformity of wind tunnel, the lift calculation may not be very affected by neglecting shear stresses [1].

Following the condition of neglecting shear stresses in the analysis, the total force can be represented in the form of pressure acting along an infinitesimal surface area of the airfoil as given in Eq. (1) [1].

$$\vec{F} = \oint -(P \cdot \hat{n}) dS \tag{1}$$

Then, the body forces can be split into its x and y components. Note, here the angle θ is the pressure force and reference body frame.

$$dF_{y'} = -P_U \cos\theta \, dS + P_L \cos\theta \; dS \tag{2}$$

$$dF_{x'} = -P_U \sin\theta \, dS + P_L \sin\theta \, dS \tag{3}$$

Then, Eq. (2-3) must be integrated to obtain the respective body force components as seen below in Eq. (4-5). Here, P_U and P_L are the local pressure readings on the upper and lower surfaces of the airfoil, respectively.

$$F_{y'} = -b \int_{x'=0}^{x'=c} (P_U - P_L) \, dx \tag{4}$$

$$F_{x'} = b \int_{y'(x'=0)}^{y'(x'=c)} (P_U - P_L) \, dy \tag{5}$$

The locations of the pressure taps along x' and y' axis specific to this experiment is given further in the next section. Local pressure coefficients can be calculated by subtracting the local pressure from the freestream pressure and diving by the freestream dynamic pressure, as given below in Eq. (6).

$$C_{p,l} = \frac{P_l - P_\infty}{\frac{1}{2}\rho_\infty U_\infty^2} \tag{6}$$

Once the local pressure coefficients along the upper and lower surfaces are known, they can be integrated to find the body force coefficients given below in Eq. (7-8).

$$C_{F_{y'}} = -\frac{1}{c} \int_{x'=0}^{x'=c} \left(C_{P,U} - C_{p,L}\right) dx \tag{7}$$

$$C_{F_{x'}} = \frac{1}{c} \int_{y'(x'=0)}^{y'(x'=c)} \left(C_{P,U} - C_{P,L}\right) dy \tag{8}$$

With the body force coefficients, the lift and drag coefficients can be calculated as a function of the angle of attack (Eq. 9-10) [1].

$$C_L = -C_{F,x'} \sin\alpha + C_{F,y'} \cos\alpha \tag{9}$$

$$C_D = C_{F,x'} \cos\alpha + C_{F,y'} \sin\alpha \tag{10}$$

III. Experimental Procedure

A. Apparatus

In this experiment, an AF100 low-speed wind tunnel is used. It is an open return suction type wind tunnel. Its structure consists of a bell-mouth diffuser at the entrance housing a honeycomb flow straightener that accelerates airflow into the test section. Due to the swirling motion of air in the room, the honeycomb flow straightener serves to reduce the lateral velocity components. The air then moves through a protective grid and variable-speed axial fan before entering the test section. The axial fan speed produces the speed within the test section and it is controlled by an electric Control and Instrumentation unit located at the rare section of the wind tunnel. The test section itself has a transparent square cross-section with dimensions of approximately 300 mm in length. There are four ports on the top of the test section – two for Pitot tubes and two for static-pressure ports. A custom-made pitot tube is mounted on the test section that moves down vertically up to 4 cm, entering the core flow region, and measuring the average freestream velocity. The pitot tube is connected to a unislide (Velmex MA4039W1-S6) that is controlled by a stepper controller (Velmex VXM-1), with its interface being connected to a computer. The LabVIEW/DTCNeX interface is used to place the control inputs [1].

Fig. 2 The AF100 Wind Tunnel [1].

The differential pressure is measured by an analog manometer that is seen on the white front panel of the wind tunnel. The pressure scanner used is the ESP-32HD which has 32 pressure ports that are connected to selected airfoil regions to record surface pressure. The data collected by the pressure scanner is converted to psig directly via DTCNeX software. This data is directly written and stored in a Microsoft Excel data file on the computer. The computer used is a Dell PC with Esterline DTCNet DAQ [1].

The airfoil used is the axis-symmetric TecQuipment NACA 0012 (Model AF102). A total of 20 points can be used to measure the local pressure on this airfoil. Fig. 5 shows the locations of these pressure taps on the airfoil, both on the top and bottom surfaces. The airfoil has a chord length of *150 mm* and a span of *300 mm*. Finally, the angle of attack is changed using a goniometric wheel installed with a 3-component force balance. Note, that the pressure ports on the airfoil are not aligned for top and bottom surfaces. The exact locations for each surface are given in the Fig 5.

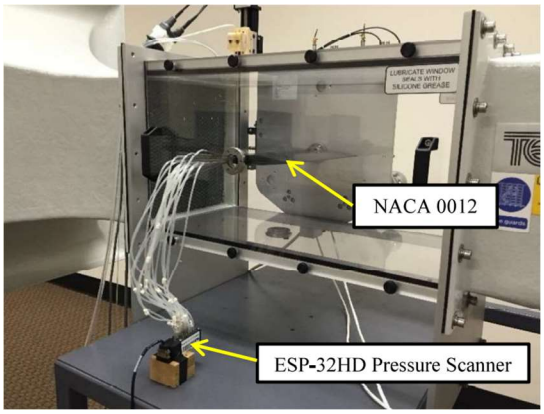

Fig. 3 The Airfoil and pressure scanner setup [1].

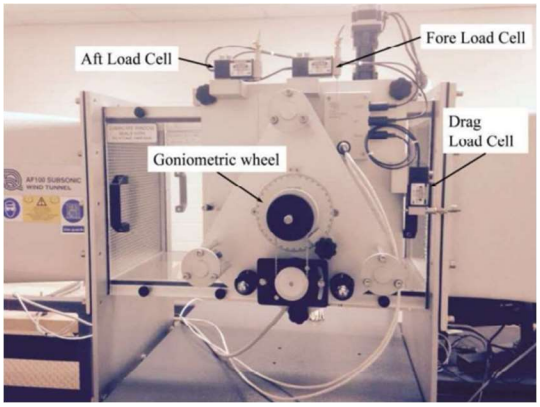

Fig. 4 The force balance with goniometric wheel [1].

B. Procedure

The experimental procedure starts with first measuring the room temperature using the thermometer attached to the room's wall followed by the measurement of room pressure using the barometer. For this experiment, the measured room temperature is **19**℃ and the room pressure is **745.5 mm of Hg**. Then, using the DTCNet DAQ, connect the DTCNeX pressure scanner interface. Open a new file on the software interface and rename the file to store data. Remember to zero the pressure scanner readings and start the angle of attack reading to zero degrees.

Once the interface recordings have been set up, start the wind tunnel and wait for the airflow to stabilize. Then record the freestream dynamic pressure reading from the analog manometer on the front white panel. The freestream dynamic pressure measured from the analog manometer for this experiment is **30 mm of H_2O**.

The airfoil is installed with white tufts (threads) on the upper and lower surfaces. The goniometric wheel is manually operated to change the angle of attack starting from 0° to 20° in 2° increments. Since the symmetric airfoil

has no camber, the direction of rotation (be it clockwise or counterclockwise) will not affect the measurements. Once the airfoil is moved high enough, the stalling behavior can be physically observed in two distinct ways: first with the aggressive movement of tufts and a high venting sound similar to a microwave vent.

Upper Surface Tapping	Distance From Leading Edge
1	0.76
3	3.81
5	11.43
7	19.05
9	38.00
11	62.0
13	80.77
15	101.35
17	121.92
19	137.16

Lower Surface Tapping	Distance From Leading Edge
2	1.52
4	7.62
6	15.24
8	22.86
10	41.15
12	59.44
14	77.73
16	96.02
18	114.30
20	129.54

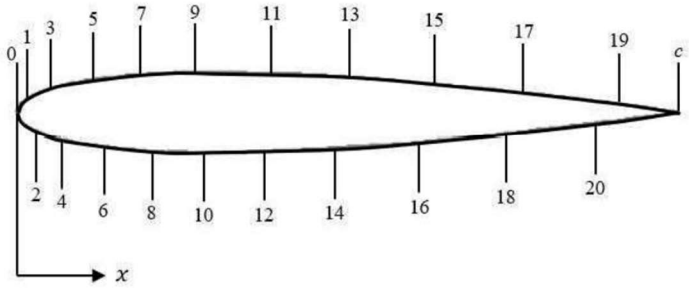

Fig. 5 Airfoil Pressure tap locations in mm [1].

C. Data Reduction Procedure

To start with data reduction, first, convert the room temperature and room pressure to metric units of kelvin (K) and pascal (Pa). The gas constant, R for air is assumed to be 287 J/kg-K. Calculate the freestream density using the ideal gas law as seen in Eq. (1). Use the room pressure, room temperature, and gas constant values for this calculation.

$$P = \rho RT \tag{11}$$

The room temperature and pressure for this experiment are recorded to be 19℃ and 745.5 mm of Hg. The conversion factor is 1 mm of Hg = 133.3224 Pa. With this information, the freestream density was calculated to be 1.185 kg/m^3.

Next, the freestream dynamic pressure from the analog manometer must be converted to pascals using the conversion factor: 1 mm of H_2O = 9.8065 Pa. For this experiment, the measured freestream dynamic pressure was 30 mm of H_2O. Using this dynamic pressure, calculate the freestream velocity using Bernoulli's equation re-arranged for velocity in Eq. (2). Here, the difference between the total pressure and freestream pressure is the freestream dynamic pressure reading from the manometer [1].

$$U_\infty = \sqrt{\frac{2(P_{total} - P_\infty)}{\rho}} \tag{12}$$

The calculated freestream velocity for this experiment is 22.279 m/s. With the freestream density and velocity known, the local pressure coefficients can now be obtained from the pressure scanner data and manometer reading.

$$P_{total} - P_\infty = P_{pitot} = 30\ mm\ of\ H_2O \tag{13}$$

The local pressure coefficient is the summation of the pressure scanner reading and pitot tube reading as seen in Eq. (14). The pitot tube reading measures the difference between total and static pressure as seen in Eq. (13). The pressure scanner readings are the difference between local and total pressure (Eq. (15)).

$$P_{local} = P_{scan} + P_{pitot} \tag{14}$$

$$P_{scan} = P_{local} - P_{total} \tag{15}$$

$$P_{local} - P_{\infty} = P_{scan} + P_{pitot} \tag{16}$$

Re-arranging the terms gives the difference between local and freestream pressure needed to calculate the local pressure coefficients at each tap location, from Eq. (16-17).

$$C_{p_l} = \frac{P_{local} - P_{\infty}}{\frac{1}{2}\rho_{\infty}U_{\infty}^2} = \frac{P_{scan} + P_{total}}{\frac{1}{2}\rho_{\infty}U_{\infty}^2} \tag{17}$$

Before calculating the local pressure coefficients, the pressure scanner data obtained in the Microsoft Excel file needs to be converted from psig to Pa using the following conversion factor: 1 psig = 6894.757 Pa. The pitot tube reading is added to each pressure data point and divided by the dynamic pressure. A suggestion would be to separate the upper and lower tap location data during this time. Additionally, in this experiment, the airfoil is moving in the anticlockwise direction due to the force balance setup. This means that during calculations, the upper surface readings (taps 1-19) given in Fig. (5) will be taken as lower surface and vice-versa. The Excel file gives pressure scanner readings in psig (taps 1-20) for an angle of attack from 0° to 20°, in 2° increments.

Once the local pressure coefficients are calculated for each surface, the data must be integrated for each angle of attack. The pressure tap locations (along the x-axis) from Fig (5) are used to calculate the change in thickness across the airfoil (along the y-axis) using Eq. (18) below:

$$\pm\frac{y}{c} = 0.60\left[0.2969\sqrt{\frac{x}{c}} - 0.126\frac{x}{c} - 0.3516\left(\frac{x}{c}\right)^2 + 0.2843\left(\frac{x}{c}\right)^3 - 0.1015\left(\frac{x}{c}\right)^4\right] \tag{18}$$

Care must be taken with the sign changes from the Eq. (18) above. The surface with pressure taps 1-19 is taken as the $-y/c$ thickness ratio and the surface with pressure taps 2-20 is taken as $+y/c$, for clarity. Once the thickness ratios are known, local pressure coefficients can be integrated using the following relations in Eq. (19-20) to obtain the forces along the body x' and y' axes.

$$C_{F_y}' = \frac{-1}{c}\int_{x'=0}^{x'=c}\left(C_{P_U} - C_{P_L}\right)dx \tag{19}$$

$$C_{F_x}' = \frac{1}{c}\int_{y'(x'=0)}^{y'(x'=c)}\left(C_{P_U} - C_{P_L}\right)dy \tag{20}$$

While performing this calculation, integrate the top and bottom surface data separately and subtract the values. This is because the pressure tap locations on the top and bottom surfaces are not aligned or equidistant. Once the integration is finished, there will only be two sets of data for the angle of attack range: C_{F_y}' and C_{F_x}'.

Using the two force coefficients, calculate the respective lift and drag coefficients for each angle of attack value using Eq. (21-22). Note, that the angles must be in radians.

$$C_L = -C_{F,x'}\sin\alpha + C_{F,y'}\cos\alpha \tag{21}$$

$$C_D = C_{F,x'}\cos\alpha + C_{F,y'}\sin\alpha \tag{22}$$

With the lift and drag coefficients known, it is easy to calculate the corresponding lift and drag forces using Eq. (23-24) below.

$$L = \frac{1}{2}\rho_\infty U_\infty^2 C_L(cb) \tag{23}$$

$$D = \frac{1}{2}\rho_\infty U_\infty^2 C_D(cb) \tag{24}$$

IV. Results and Discussion

For the data analysis part, tabulate all the lift and drag coefficients and their corresponding lift and drag forces for the angle of attack range. The calculated results for this experiment are tabulated in Table 1 below. The lift curve slope, drag coefficient versus angle of attack, and drag polar are plotted to visualize the obtained results.

Table 1. Lift, drag coefficients, and forces for the test angle of attack range.

The angle of Attack, α	Lift Coefficient, C_L	Drag Coefficient, C_D	Lift, L [N]	Drag, D [N]
0	-0.10424914	-0.00970961	-1.38013090	-0.12854340
2	0.03116133	-0.00766995	0.41253779	-0.10154069
4	0.21789511	-0.00010001	2.88466432	-0.00132398
6	0.41073691	0.01542630	5.43765354	0.20422531
8	0.54400845	0.03574914	7.20200545	0.47327480
10	0.72540048	0.06308894	9.60341373	0.83522027
12	0.83885565	0.09646067	11.10542117	1.27702111
14	0.90249069	0.13082398	11.94787117	1.73194929
16	0.72663755	0.21938957	9.61979102	2.90444917
18	0.65749287	0.24091870	8.70440023	3.18946844
20	0.62366227	0.25749070	8.25652443	3.40886147

The lift curve slope is plotted using the obtained lift coefficients and angle of attack range as seen in Fig (6). As seen, the slope increases linearly before it reaches a maximum angle of attack of 14° before decreasing non-linearly. To calculate the lift curve slope, the visible linear region at an angle of attack 2° and 10° are selected. The corresponding lift coefficients are used to calculate the slope. The lift curve slope using the chosen data points is 4.972 radians. For a symmetric, 2D airfoil, the thin airfoil theory predicts a value of $2\pi = 6.283$ radians for the lift curve slope. The difference between predicted and actual is 26.3% for this case. According to thin airfoil theory, the lift coefficient is linearly increasing with angle of attack indefinitely. It is unable to predict the stall point, also known as the point of maximum lift coefficient. This is due to its assumption of steady, inviscid, and incompressible flow. Here, the maximum lift coefficient occurs at 14° with a value of 0.902. The flow past this angle of attack begins to separate leading to stall.

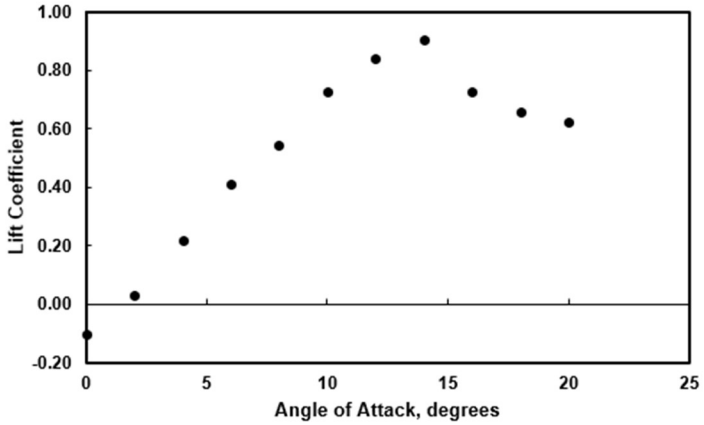

Fig. 6 Lift coefficient versus angle of attack.

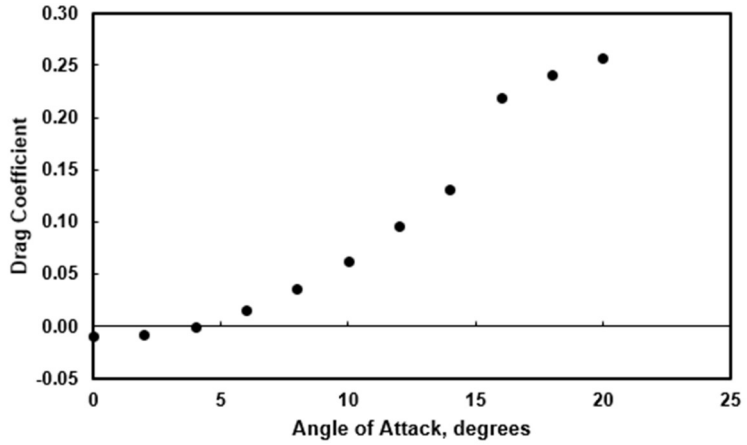

Fig. 7 Drag coefficient versus the angle of attack.

Fig. (7) shows the drag coefficient versus the angle of attack plot. The plot does not start from zero which is expected from a symmetric airfoil. It does not follow the typical trend of a symmetric airfoil. This can also be seen in the lift curve slope plot (Fig. 6) where the plot is slightly offset to the right, instead of starting at zero. Additionally, this is also observed in the drag polar below in Fig. (8) where two data points have negative values.

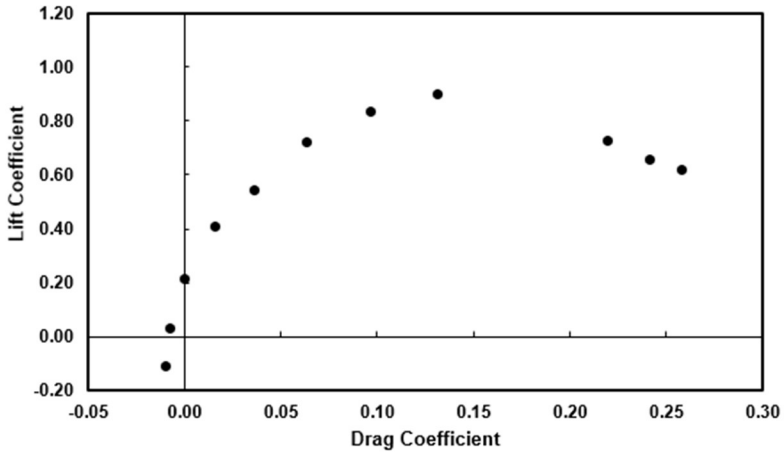

Fig. 8 Drag polar.

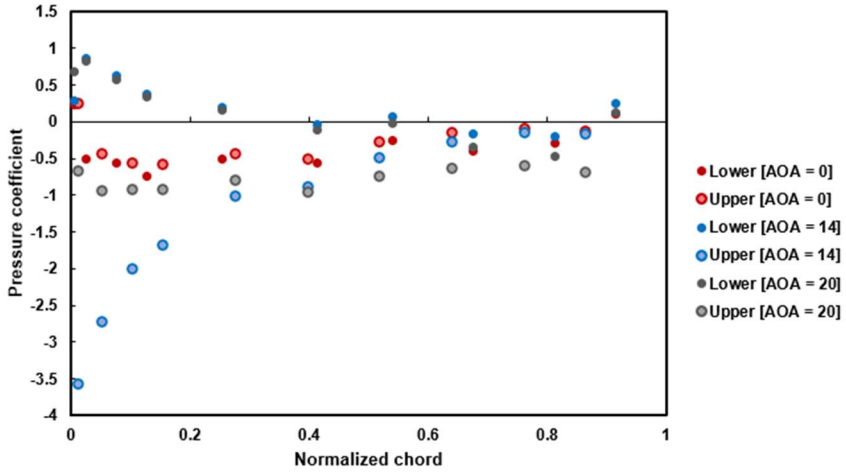

Fig. 9 Pressure coefficients on the upper and lower surface of the airfoil at selected angles of attack.

The pressure distribution plot is given in Fig. (9) for the angle of attacks of 0°, 14° and 20°. The solid datapoints denote the lower surface and the ones with outlines correspond to the upper surface. At 0° angle of attack, the upper and lower surfaces have a similar pressure distribution, slowly decreasing along the normalized chord of the airfoil. The angle of attack of 14° appears to have the largest pressure distribution difference between the upper and lower surface. The upper surface sees a large amount of pressure loss. This explains the stall point at the maximum lift coefficient at the angle of attack. Lastly, at 20° of an angle of attack, there is a considerable difference between the upper and lower pressure distributions. It is observed that the pressure loss is much lower than the stall point.

Using the data obtained during the experiment, Reynold's number can be calculated using the relation below in Eq. (25). For this calculation, the assumed dynamic viscosity μ at 19°C is $18.03 * 10^{-6}$ (N-s)/m^2.

$$Re = \frac{\rho U c}{\mu} = \frac{(1.185) * (22.279 * 0.15)}{(18.03 * 10^{-6})} = 2.20 * 10^5 \tag{25}$$

The Reynolds number is defined as the ratio between the inertial forces to viscous forces as seen in Eq. (25). Higher Reynolds numbers generally indicate turbulent flows. Additionally, a higher Reynolds number means that the flow is less viscous. The document R&M 3726 presents the results for the NACA 0012 airfoil section tested at two Reynold's numbers: $2.88 * 10^6$ and $1.44 * 10^6$. Specifically at Re = $2.88 * 10^6$, the document states the maximum lift coefficient to be unclear. One of the reasons for this uncertainty is that the flow breaks into a 3D pattern during flow separation. The maximum lift coefficient appears to be much higher, at 17.5° with a value of 1.54 for one of the cases using the Reynolds number of $2.88 * 10^6$. This means that fewer compressibility effects are present leading to higher values of lift coefficient compared to a much lower Reynolds number of $2.20 * 10^5$ obtained in this experiment [2]. With this experiment having a lower Reynolds number, it can be related to the lower value of the maximum life coefficient obtained at 0.902.

The type of drag being measured using the pressure tap measurements is the pressure drag. As mentioned earlier, the pressure sensors cannot measure wall shear stresses, hence, the friction drag cannot be calculated. Which is why they have been excluded from the analyses in this experiment.

A force balance is used to measure the forces experienced by a model placed in the wind tunnel. There are a few different types of force balances: one-component, three-component, and six-component variants. The force balance connected to the AF100 wind tunnel used in this experiment is a three-component type capable of measuring lift, drag, and sideforce. A six-component force balance can also directly measure the moments associated, namely pitch, roll, and yaw. The force balance measures the total amount of force acting on the model. Using the measurements from the pressure tap readings that exclusively measure pressure drag, in conjunction with total drag from the force balance, one can estimate the amount of skin friction drag experienced by the model [3].

The systematic errors that can be seen during the experiment can be associated with the open instrumentation port at the side of the test section. There can be a time delay between the measurements taken by the pressure scanner at the tap location and the DAQ software. From the lift curve slope graph, it is clear that the graph has shifted slightly to the right, not a characteristic of a symmetric airfoil graph. Usually, symmetric airfoils have lift curve slope plots crossing through the origin. Another source of systematic error can be from the analog manometer readings.

A pitot-static tube consists of a regular tube with additional smaller holes that circle along its surface. This device can be used to measure the drag of a body at the downstream wake region of the airfoil. The smaller holes are used to measure the static pressure while the opening of the pitot tube measures the total pressure. When using this device, the Reynolds number must be higher than 1000. The assumptions for this analysis will include steady, incompressible, and inviscid flow with a negligible elevation difference. Then, Bernoulli's equation can be used given in Eq. (26) [4].

$$p_s + \frac{1}{2}\rho V^2 + \rho g z_s \approx p_o + \frac{1}{2}\rho (0)^2 + \rho g z_0 \tag{26}$$

Here, p_s is the static pressure along a streamline, V is the velocity and z_s is the streamline's elevation. At the entrance of the pitot tube, the velocity is zero, elevation is z_0 and total pressure measured is p_o.

The control volume analysis is used to calculate the drag force acting on the airfoil. Again, the calculated force is the pressure drag. However, with this approach, the pressure taps are not required for the upper and lower surfaces since it is modeled to be inside a control volume as seen in Fig (10). Note that the control volume surrounds not only the test section but also the airfoil. The vertical plane pressure is constant along bc and gh. The pitot-static tube is placed downstream of the wake where the velocity is variable.

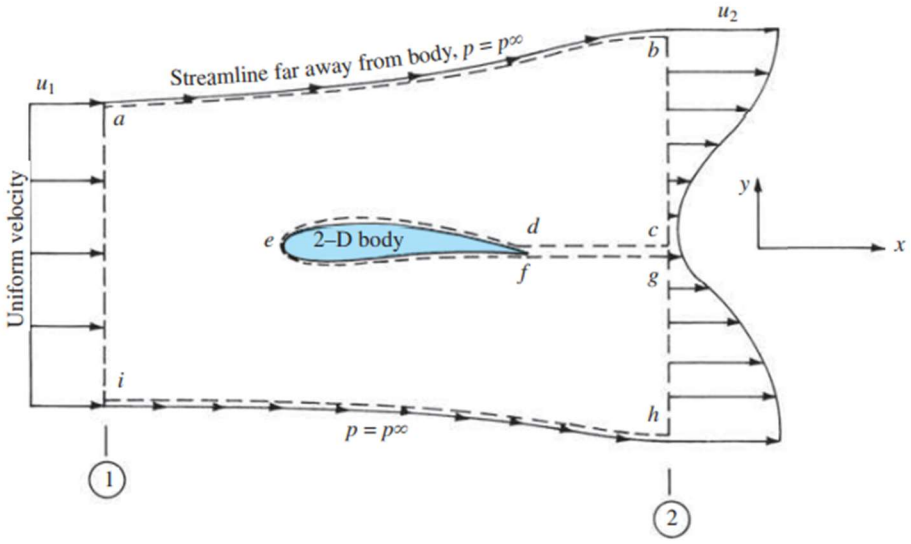

Fig. 10 Control volume analysis for a 2D airfoil [5].

Following the control volume surrounding the airfoil, the drag force can be obtained from the momentum integral used in this case, as seen in Eq. (27) below:

$$D = -\oiint(\rho V \cdot ds)u = \int_i^a \rho_1 u_1^2 dy - \int_h^b \rho_2 u_2^2 dy \tag{27}$$

Expanding on the terms using the labels *a, b, h,* and *i* for the control volume gives:

$$\int_i^a \left(p_1 + \frac{1}{2}\rho V_\infty^2\right) dy - \int_h^b \left(p_2 + \frac{1}{2}\rho u_2^2\right) dy = \frac{1}{2}D \tag{28}$$

The pressure drag can be calculated using Eq. (28) above by performing the linear momentum force balance.

V. Conclusion

In this experiment, an axis-symmetric NACA 0012 airfoil was used to measure the lift and drag forces acting along its surfaces. A subsonic AF100 wind tunnel fitted with a custom-made pitot tube and an analog manometer was used for testing. The airfoil was rotated counterclockwise from the angle of attack range of 0° to 20° in 2° increments. The airfoil was fitted with 20 individual pressure taps along the upper and lower surfaces. The location of the taps was not aligned or equidistant. Due to this chosen direction of rotation, the upper surface of the airfoil was considered to be the lower surface and vice-versa during the analysis. The pressure scanner was connected to DAQ software on a computer that collected and stored the local pressure data along each tap location for a corresponding angle of attack. The stored data was written into an Excel file for data processing.

Using the local pressure scanner data and manometer reading, the local pressure coefficients were calculated for the upper and lower surfaces, keeping consistency in the sign changes. The corresponding thickness ratios were determined for each pressure tap location. These ratios were used for integrating along the upper and lower surfaces to obtain the force coefficients acting on the airfoil for each specific angle of attack value. These force coefficients are used to calculate the lift and drag coefficients as well as the total lift and drag forces. Using these results, the lift curve slope, drag coefficient versus angle of attack, and drag polar plots are produced. Additionally, the pressure distribution for three angles of attack at plotted along the normalized chord at 0°, 14°, and 20°.

The lift curve slope calculated from the plot was 4.972 radians, with a difference of 26.3% compared to this value of 2π predicted by the thin airfoil theory. The thin airfoil theory value is higher since it does not predict the stalling point of the lift curve slope. For this experiment, the maximum lift coefficient occurs at an angle of attack of 14° with

a value of 0.902. From the pressure distributions, at this stall point the pressure gradient between the upper and lower airfoil surfaces is drastic compared to 0° and 20°. This captures the pressure loss on the upper surface during the stall. Furthermore, the stalling behavior is physically observed from the aggressive movements of the tufts attached along the surface of the airfoil and a loud whistling sound.

The Reynolds number calculated using the experiment values is comparatively lower than the values presented in the R&M No. 3726 document, which used a higher Reynolds number. This explains the reason for a lower value of the maximum lift coefficient of 0.902, while the document had values above 1. This can be linked back to the lower Reynolds number value having higher viscosity, thus lower lift due to minor compressibility effects. This experiment uses pressure scanners that are specifically useful for calculating pressure drag. Using a three-component force balance can directly measure the total drag. The difference between the total drag and pressure drag can yield skin friction drag calculation. This experiment can be further improved by using a pitot-static tube and by performing a linear momentum control volume analysis. This allows for the removal of pressure scanners along the surface of the airfoil that might contribute to surface flow disturbances.

References

[1] MAE 3182: Measurement of Aerodynamic Forces on a NACA 0012 Airfoil. The University of Texas at Arlington, Department of Aerospace and Mechanical Engineering, Fall, 2023.

[2] Gregory, N., and O'Reilly, C. L. "Low-Speed Aerodynamic Characteristics of NACA 0012 Airfoil Section, Including the Effects of Upper-Surface Roughness Simulating Hoar Frost." 1970.

[3] Force Balance. https://www.grc.nasa.gov/www/k-12/airplane/tunbal.html. Accessed Oct 9, 2023.

[4] White, F. M. *Fluid Mechanics*. McGraw Hill, 2011.

[5] Anderson, J. D. *Fundamentals of Aerodynamics*. McGraw-Hill, 2001.